

Crack front échelon instability in mixed mode fracture of a strongly nonlinear elastic solid

O. Ronsin, C. Caroli, T. Baumberger
*INSP, Université Pierre et Marie Curie-Paris 6, CNRS,
UMR 7588, 4 place Jussieu, 75005 Paris, France*
(Dated: November 1, 2018)

Mixed mode (I+III) loading induces segmented crack front échelon structures connected by steps. We study this instability in a highly deformable, strain-hardening material. We find that échelons develop beyond a finite, size-independent mode mixity threshold, markedly growing with energy release rate. They appear via nucleation of localized helical front distortions, and their emergence is the continuation of the mode I cross-hatching instability of gels and rubbers, shifted by the biasing effect of shear. This result, at odds with the direct bifurcation predicted by linear elastic fracture mechanics, can be assigned to the controlling role of elastic nonlinearity.

PACS numbers: 46.50.+a, 62.20.mm, 62.20.mt, 89.75.Kd

The question of the shape selection of a crack front propagating into a solid – hence of the resulting crack surface morphology – while central to fracture mechanics, remains up to now largely elusive. A striking example is that of fracture under (I+III) mixed mode loading. While mode I (pure tension) crack surfaces are basically planar, they generally develop, under superimposed antiplane (mode III) shear loading[1], an ”échelon” structure[2]. This can be roughly described as resulting from a crack front shape composed of a set of rotated segments connected by steep steps. Such échelon patterns are quite ubiquitous among materials : observations range from hard (glasses [3][4][5], rocks[6], metals,...) to soft (gypsum, cheese [7]) solids.

Up to now, the few theoretical attempts [4][6][8] based on standard tools of linear elastic fracture mechanics (LEFM) and an additional heuristic ansatz have not been able to predict satisfactorily such structural features as the rotation of the front segments or their spatial extension. Besides, they left untouched the issue of the existence (reported by Sommer[3], but never confirmed since) of a finite threshold amount of mode mixity for the emergence of échelon cracks. In this respect, the recent work of Pons and Karma (PK)[9], based on a phase field model of brittle fracture, constitutes an important opening. They are able to describe their results on crack propagation as a linear instability of the straight front against helical deformations, which evolve via coarsening toward the faceted shape. This has led Leblond, Karma and Lazarus (LKL)[10] to perform a linear stability analysis in the frame of LEFM. On this basis, they predict the existence of a finite threshold $(K_{III}/K_I)_c$ (where $K_{I,III}$ are the stress intensity factors imposed by the external loading) below which the planar crack remains stable. Moreover, the value of this threshold is fixed by that of the Poisson ratio only, and does not depend on the energy release rate. However, the absence of any length scale in the LEFM framework results in a pathological feature of the corresponding bifurcation: for

$(K_{III}/K_I) > (K_{III}/K_I)_c$, all wavelengths λ become simultaneously unstable, and the growth rate of the front distortion diverges as $\lambda \rightarrow 0$. As pointed by LKL, tackling the associated regularization calls for identifying a small length cutoff, the physical origin and degree of material dependence of which remain open issues.

With this question in mind, we study here (I+III) mixed mode fracture in a gelatin gel, the choice of this material being dictated by its mechanical specificities. Indeed, in this physical hydrogel, fracture proceeds via stress-induced unzipping of (triple helix) crosslinks of the gelatin network, and subsequent dissipative pull-out of the unzipped polymer chains [11]. This demands that, in the crack tip vicinity, stresses build up to a level $\sim 100E$, with E the small strain Young modulus. As discussed by Hui [12], such a level of stress concentration, while prohibited in linear elastic materials by elastic blunting, can be reached in soft polymer gels thanks to the huge strain hardening signaling the crossover between the coiled (entropic) and taut chains (enthalpic) elastic regimes. The extension of the near-tip region where non linearities become relevant naturally provides a small scale cutoff ℓ_{NL} below which the universal inverse square root LEFM stress divergence no longer holds, as directly demonstrated by Livne *et al* [13]. Estimating this length as the distance to the tip where the LEFM stress reaches a value $\sim E$ leads, in agreement with ref.[14], to $\ell_{NL} \sim \mathcal{G}/E$, with \mathcal{G} the fracture energy. In hydrogels ℓ_{NL} typically lies in the $100\mu\text{m}$ – 1mm range [15][16], much larger than both the process zone and network mesh sizes. It can thus be expected to play a decisive role in crack path selection. Indeed, it has been shown to govern the oscillatory instability in rapid fracture of brittle gel films [16] as well as the crack branching response of gelatin gels to a solvent-induced environmental shock [17].

Extensive exploration of crack surface morphologies in the quasi-static regime reveals the existence in our system of a finite mode mixity threshold which, at variance with the LKL prediction, strongly increases with

\mathcal{G} . Moreover, we bring direct evidence that the emergence of the échelon structures does not follow the linear-instability-plus-coarsening PK picture. Rather, they develop via a mechanism akin to the emergence of the cross-hatching (CH) instability observed in mode I fracture of gels [15][18] and rubbers [19] – namely, the localized nucleation of steps triggered by structural fluctuations whose minimum amplitude decreases as K_{III}/K_I grows. From this we conclude that, in the presence of large elastic crack tip blunting, the mixed mode fracture response is fully controlled by non-linearities. We then argue that, more generally, the relevance of the LKL linear stability analysis should be correlated with the amplitude of mode I crack surface roughness.

Our experiments are performed, according to the protocol described in ref [20], on gel slabs ($E = 12\text{kPa}$) made of 5 wt% gelatin in a water-glycerol mixture. Sample sizes and compositions are listed in Table I. Mixed mode loading is introduced by notching the sample, previously stretched to the desired level, at an angle θ_0 (see Fig.1) from the plane of propagation of pure mode I cracks. Profilometric analysis of crack surfaces is performed as described in the Supplemental Material [21].

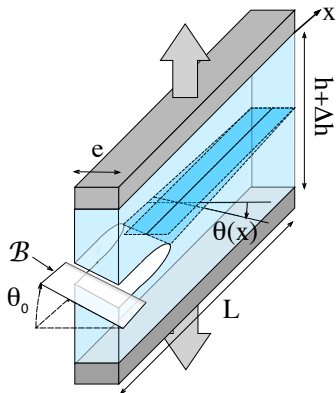


FIG. 1. Sketch of the experimental setup: the gel slab (unstrained dimensions $L \times h \times e$), once stretched by Δh , is notched at angle θ_0 by the blade \mathcal{B} .

We choose for our control parameters (i) the mode mixity indicator $m_0 = \tan \theta_0$ (which would measure K_{III}/K_I in the $e \rightarrow \infty$ limit), with θ_0 ranging up to 50 deg. (ii) the initial energy release rate $\mathcal{G} = \mathcal{W}(Le/\cos\theta_0)^{-1}$, with \mathcal{W} the loading work. Fracture of gelatin being highly dissipative, in the explored loading range ($\mathcal{G} < 20 \text{ J.m}^{-2}$), mode I crack propagation is steady and quasistatic (velocities $V \lesssim$ a few mm.s^{-1})[11].

Our results on crack surface morphologies are summarized on Fig.2, which gathers data from the (L, e, h, η) sets listed in Table I. In agreement with previous works, we observe that mode III induces échelon cracks. However, we find that they only appear beyond a finite mode mixity threshold m_c (dashed line on Fig.2), thus con-

TABLE I. Gel sample characteristics. Slab dimensions (in cm) as defined on Fig.1. η (in mPa.s) is the viscosity of the water-glycerol solvent.

slab symbols	L	h	e	η
diamonds	30	3	1	11
squares	30	3	1	3.6
circles	30	3	2	11
down triangles	30	10	1	11
up triangles	20	2	0.5	11

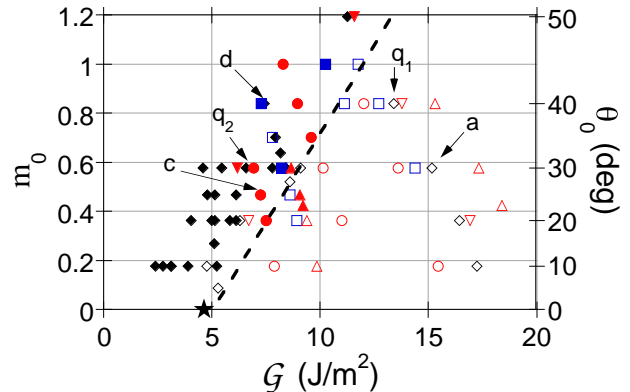


FIG. 2. Crack surface morphology, in the (energy release rate \mathcal{G} , mode mixity indicator m_0) control parameter plane for samples with various sizes and solvent compositions. Symbol shapes are defined in Table I. Empty symbols: smooth cracks; Full symbols: échelon cracks. The dashed line defines the échelon instability threshold $m_c(\mathcal{G})$. The star symbol corresponds to the onset of the mode I cross-hatching instability (see text). Labels a, c, d refer to Figure 3. For q_1, q_2 see text.

firming Sommer's suggestion [3]. Strikingly, the domain of existence of échelon fronts in the (m_0, \mathcal{G}) parameter space turns out to be insensitive to both the slab geometry and the solvent viscosity. However, m_c is not a constant but grows markedly with \mathcal{G} . As m_0 is increased, the fracture behavior evolves as follows.

Smooth regime: At small notch angles ($m_0 < m_c$), the crack front remains quasi-linear [21]. However, as it propagates, its tilt angle $\theta(x)$ decreases steadily until it returns to the mode I configuration. Indeed, we meet here with the difficulty inherent to mixed mode fracture experiments - namely it is in practice impossible to impose a steady mode mixity amount. Here, as in refs [4][5], we only impose its initial value. A crack surface typical of this smooth regime is shown on Fig.3.a. Profile analysis for samples with various θ_0 and e values (see Fig.3.b) shows that the tilt angle relaxation curves obey the scaling law: $m(x) = m_0 f(x/e)$, where f exhibits an exponential-like decay over a range $x/e \simeq 1$: in agree-

ment with Saint-Venant’s principle, the memory of initial conditions is constrained by the sample geometry[22]. Finally, closer examination reveals (insert of Fig.3.b), on top of the global smooth profile, a roughness of micrometric r.m.s. amplitude with the same characteristics as that of mode I crack surfaces.

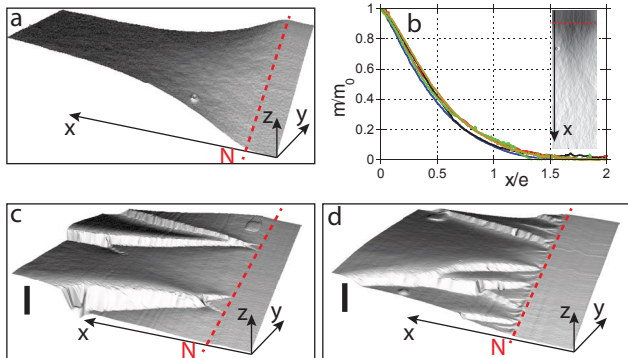


FIG. 3. Crack surface morphologies for parameter values as labeled on Fig 2. (a): Surface profile of a smooth crack (area $6 \times 24 \text{ mm}^2$). (b) Scaled mode mixity parameter (m/m_0) vs scaled propagation distance (x/e) from notch line N, for: $\{e = 1 \text{ cm}, m_0 = 0.27, 0.36, 0.58, 0.84\}$ and $\{e = 2 \text{ cm}, m_0 = 0.36\}$. *Inset*: Microroughness of crack (a) as revealed by grazing angle illumination. (c,d): Surface profiles of cracks close beyond threshold (c), and deeper into the échelon regime (d) (areas $8 \times 10 \text{ mm}^2$, vertical bar $500\mu\text{m}$).

Echelon regime: For $m_0 \gtrsim m_c(\mathcal{G})$ (Fig.3.c), the fracture surfaces exhibit highly localized steps, oriented so as to reduce the tilt of the facets which join them. They nucleate at the very tip of the notch and grow, as the crack propagates, up to heights $\sim 100\mu\text{m}$. Moreover, we find that they systematically drift along the front, in a seemingly random direction. As m_0 gets larger (Fig 3.d), the step density increases and we observe step “collisions” which result in their merging (Fig 3.a,b). Thanks to the drift, the steps successively exit from the slab, thereby relaxing the average tilt angle and finally leaving a smoothed crack surface.

Let us now put this set of results in regard to the instability scenario emerging from refs.[9][10]. While we do agree with LKL on the existence of a finite mode mixity threshold, we notice two main discrepancies:

(i) At variance with their prediction of a \mathcal{G} -independent m_c value ($\simeq 0.23$ for our quasi-incompressible gel) we measure a tenfold increase when \mathcal{G} grows by a factor ~ 2 . Note that, since we find that $m_c(\mathcal{G})$ is independent of sample thickness, this difference cannot originate from a mere finite size effect.

(ii) PK suggest that échelon patterns emerge via a linear instability as a quasi sinusoidal front modulation which then coarsens as it amplifies, according to a direct bifurcation picture. We observe a markedly different be-

havior, namely nucleation and growth of highly localized front distortions.

These discrepancies raise an obvious issue: could nucleation, in our experiments, be heterogeneous, i.e. triggered by defects imprinted by the notching blade? In order to address this question, we have performed the following “mechanical quench” experiment: we initiate a crack in the smooth regime (point q_1 on Fig.2), let it propagate over a distance of 1.2 mm, then suddenly reduce the remote tensile loading, thus bringing the crack into the échelon regime (point q_2). Fig 4.a shows the corresponding surface profile. Unambiguously, the steps nucleate quasi-simultaneously and without measurable delay on the quench line Q. Moreover, as illustrated on the blow-up Fig 4.c, they emerge from ridges of the microroughness already present in the pre-quench, nominally smooth, NQ region. On the other hand, we find (see Fig.4.b) that this microroughness exhibits no discernible correlation with the blade-generated grooves. We therefore conclude that the échelon instability develops via homogeneous nucleation of localized structures.

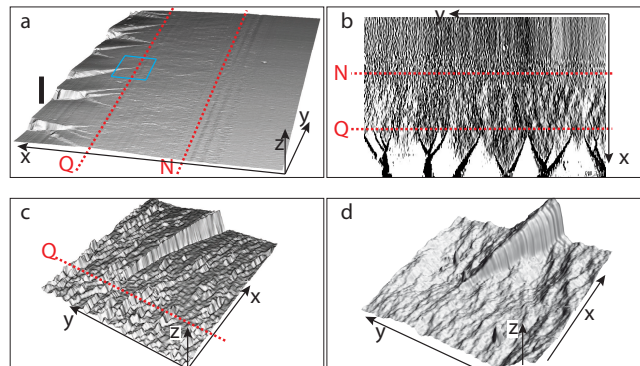


FIG. 4. (a): Surface profile corresponding to the quench protocol (see text): N indicates the notching line, Q corresponds to the position reached by the smooth crack front at the time of the mechanical quench (area $5 \times 3.3 \text{ mm}^2$, vertical bar $300 \mu\text{m}$). (b) Same data plotted under simulated grazing illumination showing grooves left by the notching blade (above N), smooth crack microroughness (region NQ) and échelon emergence (below Q). White regions are facing the light source. (c) Blow up of the square area marked on (a), showing nucleation and growth of an échelon step (area $500 \times 500 \mu\text{m}$, peak-to peak $20 \mu\text{m}$). (d) (Adapted from Baumberger *et al.* [15]) Nucleation and growth of a cross-hatching defect emerging on the surface of a mode I crack (area $400 \times 400 \mu\text{m}$, peak-to peak $15 \mu\text{m}$).

This phenomenology is highly reminiscent of that of the Cross-Hatching (CH) instability previously observed in mode I fracture of highly deformable materials and analyzed, on the case of gelatin, in ref.[15]. This latter instability is characterized by the emergence, below a critical energy release rate \mathcal{G}_{CH} , at random locations across the slab width, of narrow steps drifting in either

direction. We have interpreted them as the response of the crack front to transient pinning by a toughness fluctuation: this gives rise to a local (I+II+III) mixed mode configuration, hence to a helicoidal self-amplifying front deformation evolving into two connected half-cracks. The resulting, symmetry-breaking, local morphology is thus akin to the (I+III) échelon one, while the global symmetry imposed by the absence of remote shear loading reflects into the random sign of the facet tilt angles.

As immediately appears when comparing Figs.4.c,d, échelon and CH steps develop in a strikingly similar way. This suggests that, in our soft elastic system, the échelon instability might be the continuation of the CH one, that would be simply shifted under the biasing effect of shear loading. If such is the case, the échelon threshold line $m_c(\mathcal{G})$ must extrapolate to G_{CH} in the $m_0 = 0$ (pure mode I) limit. For the gels studied here, we measure a G_{CH} value of $4.6 \pm 0.3 \text{ J.m}^{-2}$, in agreement with [15]. As seen on Fig.2, we find that this value is fully compatible with the extrapolation of the échelon threshold line. Let us moreover note that $m_c(\mathcal{G})$ turns out to be insensitive to a threefold variation of the solvent viscosity η , in agreement with the η -independence of G_{CH} [15].

In summary, we are able to assert that, as far as the échelon instability is concerned, the effect of a finite mode mixity amount is merely to facilitate the local development of helical defects generated on front pinning tough sites provided by the intrinsic disorder of the random polymer gel network.

This conclusion may at first sight appear quite puzzling. Indeed, it points to the irrelevance to our system of the linear instability-plus-coarsening scenario. If such is the case, why is the (formally indisputable) LKL linear analysis not valid here or, in other words, what is the criterion for its validity?

With regard to this question, it is important to note that, as shown in [15], the in and out of plane front deviation amplitudes for a fully developed CH defect turn out to be on the order of the cutoff length ℓ_{NL} associated with elastic non-linearities. In other words, the nucleation and initial development of such defects take place in the elastically blunted, fully strain-hardened, tip vicinity. Hence the fact that LEFM cannot account for these processes.

Nevertheless, as discussed above, the LKL approach should be legitimate on length scales larger than ℓ_{NL} , and the spatially extended destabilization which it predicts might compete with the biased CH process. Let us stress, however, that this extended response must be understood as driven by the noise *renormalized up to the coarse-graining scale*. Now, as the LEFM front problem is itself non-linear, the front deformation as calculated by LKL is the first term of an amplitude expansion, and truncation to first order is valid only for noise amplitudes below some cutoff A_{max} fixed by the precise expression of next order terms. Note that A_{max} should exhibit a uni-

versal dependence on the small strain elastic coefficients. On the other hand, the coarse-grained noise amplitude scale $\bar{A}(\ell_{NL})$, which can in principle be evaluated from the micro-roughness spectrum of mode I cracks, certainly depends on nonlinear (elastic, plastic) material properties. We believe our strongly nonlinear elastic system to correspond to the regime $\bar{A}(\ell_{NL}) > A_{max}$ in which the extended instability is irrelevant.

These remarks clearly suggest the validity of the LKL scenario to be material dependent and, hence, the nature of the échelon instability itself to be a non-universal feature. Insofar as calculating higher orders terms of the LEFM amplitude expansion appears quite a formidable task, we hope that it will be possible to test this proposition by extending the phase field approach to include nonlinear elasticity.

We are grateful to A. Karma, V. Lazarus, K. Ravi-Chandar for stimulating discussions and to H. Henry for communication and discussion of unpublished results.

-
- [1] B. Lawn, *Fracture of Brittle Solids*, 2nd Ed. (Cambridge, University Press, 1993).
 - [2] D. Hull, *Fractography* (Cambridge, University Press, 1999)
 - [3] E. Sommer, *Eng. Frac. Mech.*, **1**, 539 (1969).
 - [4] Bisen Lin, M.E. Mear and K. Ravi-Chandar, *Int. J. Frac.*, **165**, 175 (2010).
 - [5] V. Lazarus, F.-G. Buchholz, M. Fulland and J. Wiebesiek, *Int. J. Frac.*, **153**, 141 (2008) and references therein.
 - [6] M.L. Cooke, D.D. Pollard, *J. Geophys. Res.*, **101**, 3387 (1996).
 - [7] R.V. Goldstein and N.M. Osipenko, *Doklady Phys.*, **57**, 281 (2012).
 - [8] V. Lazarus, J.B. Leblond, S.E. Mouchrif, *J. Mech. Phys. Solids*, **49**, 1421 (2001).
 - [9] A.J. Pons and A. Karma, *Nature*, **464**, 85 (2010).
 - [10] J.B. Leblond, A. Karma and V. Lazarus, *J. Mech. Phys. Solids*, **59**, 1872 (2011).
 - [11] T. Baumberger, C. Caroli, D. Martina, *Nature Materials*, **5**, 552 (2006).
 - [12] C.Y. Hui, A. Jagota, S.J. Bennison, and J.D. Londono, *Proc. R. Soc. London, A* **459**, 1489 (2003).
 - [13] A. Livne, E. Bouchbinder, I. Svetlitsky, *J. Fineberg, Science*, **327**, 1359 (2010).
 - [14] P.H. Geubelle and W.G. Knauss, *J. Elast.*, **35**, 61 (1994).
 - [15] T. Baumberger, C. Caroli, D. Martina and O. Ronsin, *Phys. Rev. Lett.*, **100**, 178303 (2008).
 - [16] T. Goldman, R. Harpaz, E. Bouchbinder, and J. Fineberg, *Phys. Rev. Lett.*, **108**, 104303 (2012).
 - [17] T. Baumberger and O. Ronsin, *Eur. Phys. J. E*, **31**, 51 (2010).
 - [18] Y. Tanaka, K. Fukao, Y. Miyamoto, and K. Sekimoto, *Europhys. Lett.*, **43**, 664 (1998).
 - [19] A.N. Gent and C.T.R. Pulford, *J. Mater. Sci.*, **19**, 3612 (1984).
 - [20] T. Baumberger, C. Caroli, and D. Martina, *Eur. Phys. J. E*, **21**, 81 (2006).
 - [21] See Supplemental Material.

- [22] Observation by H. Henry (private communication) of the same scaling behavior in phase field simulations of brittle fracture confirms its purely geometric origin.

Supplemental Material: Crack front échelon instability in mixed mode fracture of a strongly nonlinear elastic solid

O. Ronsin, C. Caroli, T. Baumberger

Profilometric analysis of crack surfaces: In order to circumvent sample evolution induced by solvent evaporation, we make replicas of the fresh fracture surfaces by casting and UV-curing thin layer of glue. The replicas are fixed on a two-axes x-y translation stage and scanned with the help of a confocal chromatic optical sensor (Micro Epsilon NCDT IFS 2401-1). The sensor itself is fixed to a z translation stage so as to extend its nominal 1 mm measuring range up to 2 cm. This home-built profilometer enables us to scan zones of typical areas $1 \times 5 \text{ cm}^2$ with a vertical resolution of 100 nm and a lateral one of $10 \times 10 \mu\text{m}^2$. Note however that, due to the need for glue trimming along the replica edges, the scanning zone only extends up to a distance of 1mm from each edge.

While the tilt angle $\theta(x)$ is defined as the inclination of the front line in the stretched sample, with respect to the sample (horizontal) mid-plane, profile measurements are performed on the unloaded surfaces. In order to identify the $\theta = 0$ reference plane, all experimental runs are continued up to propagation distances such that the crack has returned to the mode I configuration. From the value $\alpha(x)$ of the measured tilt angle we infer $\theta(x)$ according to:

$$\theta(x) = \tan^{-1} \left[\left(1 + \frac{\Delta h}{h} \right)^2 \tan \alpha(x) \right]$$

which accounts for the affine deformation of the incompressible slab due to the grip displacement Δh . We have checked that we thus recover the value θ_0 of the notching angle up to $\pm 5\%$.

Profiles in the smooth regime: Figure S₁ shows sections $h(y)$ of a “smooth” fracture surface by planes perpendicular to the propagation direction x . As analyzed in reference [Bisen Lin, M.E. Mear and K. Ravi-Chandar, *Int. J. Frac.*, **165**, 175 (2010)], finite slab thickness induces a mode II loading component which decreases gradually from the edges and vanishes on the mid-plane $y = 0$. Although we cannot access the immediate vicinity of the edges (see above), one indeed clearly distinguishes on Figure S₁ the bending trend expected to result from this effect. We choose to define the tilt angle from the slope of the profile at $y = 0$. We then compute with the help of the above equation the local mode mixity indicator $m(x) = \tan \theta(x)$, whose evolution is shown on Fig. 3b for cracks in the smooth regime.

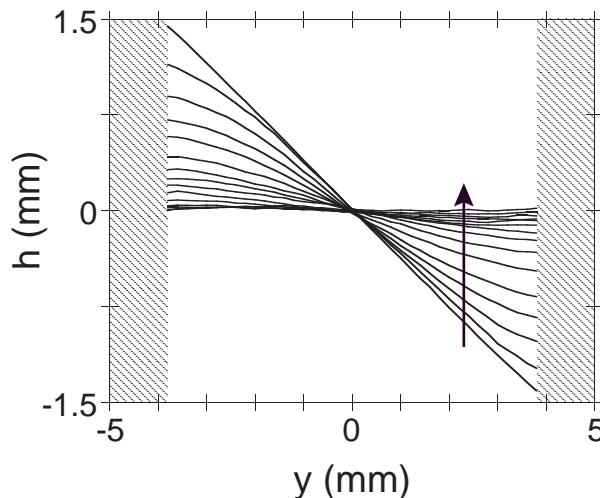


Fig. S₁: Sections of the smooth fracture surface shown on Fig. 3a, by planes perpendicular to the propagation direction x and evenly spaced ($\Delta x = 2 \text{ mm}$) from the initial straight notch, growing in the direction of the arrow. The hatched stripes indicate the edge regions of the 10 mm wide sample inaccessible to scanning.